Recent Developments in the Theory of Supralattices

Alexander A. Demkov* and Otto F. Sankey

Department of Physics and Astronomy and Materials Research Group, Arizona State University, Tempe, Arizona 85287

Received February 14, 1996. Revised Manuscript Received May 21, 1996[⊗]

Regular 3D arrays of nanosize clusters can be synthesized in the cages of zeolite frameworks. Such nanocomposites are known as *supralattices*. The appeal to use zeolites mainly comes from the periodic nature of channels and cages in these structures. Alumino−silicate zeolite frameworks have wide electronic bandgaps and are transparent, which opens up the possibility of forming new guest electronic states within the gap. Revolutionary developments in methods of electronic structure theory make possible the quantitative investigation of such complex systems as *supralattices*. We discuss recent advances in theoretical methods based on the electronic structure theory and describe several recent applications of these techniques to supralattices. Theory can help answer questions as to what kind of guests are appropriate for a given host and what are the energetics and dynamics of the cluster formation in the zeolite cages. Optical, magnetic, and thermal properties of the resulting composite can now, in some cases, be predicted. As examples, we discuss alkali metals in Si clathrates, sodium−sodalite, zeolite Na-Y, and silicon clusters in silica−sodalite. We emphasize the fundamental aspects of these problems.

I. Introduction

Supralattices, or cluster solids, are nanocomposites consisting of a framework "host" material used to support a 3D periodic arrangement of small atomic clusters, molecules, or polymers also known as "guest" species. Typically, zeolite materials are chosen as the host material. The large zeolite cages, from several tens to a few angstroms across, offer lodging sites to self-assemble and stabilize clusters within the zeolite framework. These regularly spaced nanosize clusters have the geometry of either that of a free cluster, bulk fragment, or completely new structures stabilized by the zeolite framework. However, as we shall illustrate below, other materials with "caged" structures may be also used to form supralattices. The properties of the resulting composites are expected to be quite different from those of both the host material and the guest species.

Packaging with three-dimensional crystalline periodicity produces well-defined structures with optical, magnetic, and electronic properties tunable upon the chemical modification of the system. Novel nanostructures with two- and three-dimensional confinement unaccessible via conventional methods of synthesis offer possibilities of creating new materials of both scientific and commercial interest.[1] Recent literature has tended to emphasize the practical aspects, including the discussion of the properties for specific applications, and it seemed therefore useful in this review to stress some of the fundamental aspects. Supralattices give us a unique opportunity to study some of the very basic questions of materials physics and chemistry. Among these questions are the process of cluster formation, the behavior of small clusters under "pressure", the optical properties of spatially confined systems, and a whole family of many-body effects such as the metal-to-insulator transition and correlated electron magnetism, to name a few. The zeolite doping is particularly interesting in the study of electron correlation effects because both the one-electron and the many-body interactions can be tuned by altering either the concentration of guests or the "chemistry" of the framework. It is the purpose of this paper to review some of the recent results in the theory of these novel materials, as well as to introduce to a broader audience of materials scientists new developments in the theoretical tools currently available.

II. Hosts and Guests

Zeolites are framework structures which are open in the sense that they contain large polyhedral cages of atoms connected to each other by channels. The tetrahedral atom (*T* atom) is usually Si and is surrounded by four oxygen atoms. Commonly the element Al is substituted for some of the Si atoms. In these aluminosilicates an additional cation (e.g., Na) is incorporated interstitially within the lattice and its electron is donated to the Al site to satisfy the bonding requirements of a tetrahedral framework. Smith[2] defines a zeolite as a crystalline aluminosilicate with a 4-connected tetrahedral framework structure enclosing cavities occupied by large ions and water molecules, both of which have considerable freedom of movement, permitting ion exchange and reversible dehydration. However, synthetic zeolites include numerous examples that do not meet one or more of these criteria. Synthetic zeolites play a major role in petrochemical catalysis, and also are widely used in radioactive waste storage, water treatment, gas separation and purification, and animal feed supplements—all because of their exceptional abilities for ion-exchange and sorption.[3] Zeolite frameworks offer a unique opportunity for creating new three-dimensional supralattices, i.e., artificial periodic lattices of clusters or "quantum dots" of semiconducting (or

[⊗] Abstract published in *Advance ACS Abstracts,* July 1, 1996.

S0897-4756(96)00124-X CCC: $12.00 © 1996 American Chemical Society

other) materials whose dimensionality and electronic properties can be partially controlled.

There has been considerable experimental effort in this field, and several new zeolite-based supralattice materials have been synthesized. The first work originated in the Soviet Union when Bogomolov et al.[4] incorporated Se in zeolite X and Z. They find that Se chains self-assemble in the channels, and the optical absorption threshold shifts upward into the blue region compared to chainlike bulk trigonal Se. This exciting observation suggested that "quantum confinement" produces major changes of the electron states in this system—this effect is similar to the quantum confinement that occurs in layered semiconductor superlattices but is an order of magnitude larger!

Many subsequent experiments have incorporated clusters into the framework, and the optical absorption threshold generally shows the "quantum confinement" blue-shift. As specific examples we mention CdS[5] clusters in zeolites, GaP in zeolite Y,[6] Se in mordenite,[7,8] Se in zeolites A, X, Y, AlPO-5, and mordenite,[9] Na clusters in sodalite,[10] PbS,[11] Pt,[12] Na–Cs alloys,[13] and K clusters in zeolite A and X.[14] This is only a partial list, and further examples can be found in review articles by Stucky et al.[15] and Ozin et al.[16] Part of this effort has been motivated by applications to nonlinear optical devices and solar elements, since the $Al_{1-x}Si_xO_2$ aluminosilicate matrix has a wide bandgap (transparent).

III. Overview of Theoretical Methods

Imagine that we need to design a nanocomposite with certain properties. First we will have to select the host material that meets our requirements and is stable for the environment of the particular application. Then, just as if we were designing a laser, we should choose the active guest species. Finally, we would need to know whether we can put the guest inside the cages of the host matrix and make sure that possible guest–host interections do not destroy the desirable properties of our "smart material". Some form of theoretical modeling appears to be extremely useful to address some of the questions raised in making educated choices for any of the above.

What are our requirements to the model? It must be able to describe both the zeolite (or other) framework and the guest cluster as well as possible interactions between the two. In addition, if we are looking for a material to be used in electronic, optic, or magnetic applications, we need to evaluate these quantum properties of the resulting composite as well. The first question is, where do the atoms go? And once we know the atomic geometries we must be able to calculate the relevant physical properties. Sometimes we actually know very well where the atoms are (let us say from X-ray data) and desire to understand some important aspects of the electronic structure, e.g., to interpret the optical absorption. Obviously, it would be very desirable to have a unique systematic approach to handle all of the possible cases. However, real life is always far more complex than the best of any of our models. Fortunately, theory combined with certain physical intuition allows us to choose models describing the most important features of the system, albeit on a case-to-case basis. We shall now mention some of the most useful theoretical tools with the emphasis on the recent developments and applications to zeolite supralattices.

Once we have adopted an atomistic picture, there are two fundamental options on how we describe the interatomic interactions—it can be done classically (through empirical force fields) or quantum mechanically (solving the Schrödinger equation for the electrons). We will initiate our discussion with the "correct" quantum picture of the solid and later touch on the classical force field methods. The solid is an assembly of ions (heavy positively charged particles) and electrons (light negatively charged particles) interacting with each other via Coulomb forces. The total energy is obtained from the Hamiltonian operator of interacting ions and electrons:

$$\hat{H} = \sum_{\text{electrons}} \frac{p_i^2}{2m} + \sum_{\text{ions}} \frac{P_l^2}{2M_l} + \frac{1}{2}\sum_{l,l'} \frac{Z_l Z_{l'}}{|\vec{R}_l - \vec{R}_{l'}|} + \frac{1}{2}\sum_{i,j} \frac{e^2}{|\vec{r}_i - \vec{r}_j|} - \sum_{l,i} \frac{Z_l e}{|\vec{r}_i - \vec{R}_l|} \quad (1)$$

where the first two terms are the kinetic energies of electrons and ions, the third and the fourth terms are the ion–ion and electron–electron repulsion, respectively, and the last term is the electron–ion attraction.

The first approximation is to decouple electrons from ions by taking the advantage of the enormous difference of the time scales for the ionic and electronic motion. This is done within an *adiabatic* or *Born–Oppenheimer approximation*:[17]

$$\Psi_{l,n}(\{R\},\{r\}) = \Phi_l(\{R\},\{r\})\chi_{\lambda,n}(\{R\}) \quad (2)$$

Here $\Phi_\lambda(\{R\},\{r\})$ is an eigenstate of the electronic problem for some "frozen" configuration of the nuclei $\{R\}$

$$\left(\hat{H} - \sum_{\text{ions}} \frac{P_l^2}{2M_l}\right)\Phi_\lambda(\{R\},\{r\}) = \epsilon_\lambda(\{R\})\Phi_\lambda(\{R\},\{r\}), \quad (3)$$

and functions $\chi_{\lambda,n}(\{R\})$ are the eigenstates of the nuclear "vibrational" problem:

$$(\sum_{\text{ions}} (P_l^2/2M) + \epsilon_\lambda(\{R\}))\chi_{\lambda,n}(\{R\}) = \epsilon_{\lambda,n}\chi_{\lambda,n}(\{R\}) \quad (4)$$

The ansatz (2) neglects all the electron transitions due to the ionic motion (that is why the approximation is called *adiabatic*); instead, an electronic state itself is deformed by the ionic displacement. The full discussion of this problem would, however, take us well beyond the intended scope of this section. In this work, we will not be concerned with the quantum aspects of the ionic motion, and from now on we shall consider the ionic motion to be classical, and the particles to move in the potential $\epsilon_0(\{R\})$, where $\epsilon_0(\{R\})$ is the electron ground-state energy for a frozen nuclear configuration.

The potential function $\epsilon_0(\{R\})$, once it is known, enables us to obtain the complicated many-body forces with which atoms interact with each other. From the energy and forces, one can answer a great number of questions about the system under consideration, such as the equilibrium structure, phase transitions, electronic and thermal properties, etc.

In the empirical classical potential (or force field) model, an educated guess is made about the exact form of the potential function $\epsilon_0(\{R\})$. A first approximation is to obtain it as a sum of pair interatomic potentials $V(r_{i,j})$, where $r_{i,j}$ is the distance between the atoms:

$$\epsilon_0 = \frac{1}{2}\sum_j \sum_j V(r_{i,j}) \tag{5}$$

or by a more sophisticated function such as including 3-body, $V(r_i,r_j,r_k)$ or higher contributions. Once the form of the potential function is chosen, the Newtonian equations of motion

$$-\nabla_i \epsilon_0(\{R\}) = \vec{F}_i = M_i \vec{a}_i \tag{6}$$

are integrated using a Gear, Verlet,[18] or other algorithm. There are many interatomic potentials available[19−21] for SiO_2, and for a comprehensive review of these techniques we recommend an excellent book by Catlow et al.[22] or a recent review by Sauer.[23] The difficulty with potentials is that they generally need input data for which the potential must be fit. In some cases such as aluminosilicates, such data exists. But if a cluster is incorporated into the lattice, one cannot be sure what the lattice−cluster interaction parameters are.

The electronic structure method is a quntum mechanical method to obtain ϵ_0 ($\{R\}$). It is, however, an impossible task to solve the Schrödinger equation for 10^{23} interacting particles! Near-exact solutions for very small systems by means of quantum Monte Carlo methods have recently become available.[24] Unfortunately, the majority of practical problems cannot be solved by such exact techniques and must be solved by means of approximate theories. Historically, chemists have tended to use Hartree−Fock methods, while physicist have prefered the density functional theory of Hohenberg, Kohn, and Sham.[25,26] Density functional theory is in principal exact, but practical applications are always approximate. A review of Hartee−Fock calculations can be found in recent papers by Silvi and Hess.[27,28] We next briefly review the density functional method.

A. Density Functional Theory. Hohenberg and Kohn[25] showed by reductio ad absurdum that $v(\vec{r})$ (the electron potential) is a unique functional of $\rho(\vec{r})$ (the electron density), and therefore the full many-body ground state is a unique functional of $\rho(\vec{r})$. They introduced the energy functional for the ground state:

$$E_v(\rho) = \int v(\vec{r})\,\rho(\vec{r})\,\mathrm{d}\vec{r} + \frac{1}{2}\int\frac{\rho(\vec{r})\,\rho(\vec{r}\,')}{|\vec{r}-\vec{r}\,'|}\,\mathrm{d}\vec{r}\,\mathrm{d}\vec{r}\,' + G[\rho] \tag{7}$$

where $G[\rho]$ is a universal functional, valid for any number of electrons in any external potential. They also showed that the $E_v(\rho)$ satisfies a variational principle and assumes its minimum for the ground-state density $\rho(\vec{r})$ (the usual constraint of the particle conservation was applied). The universal functional $G[\rho]$ contains the kinetic, exchange, and correlation energies. Unfortunately, the exact form of the functional $G[\rho]$ for the general case is still unknown.

Kohn and Sham (KS)[26] proposed the following scheme to solve the minimization problem. An auxiliary independent electron problem is introduced. The auxiliary trial potential generates an electron density in the following sense. Consider the Schrödinger equation

$$\left[-\frac{1}{2}\nabla + [\phi(\vec{r}) + \mu_{xc}(\rho(\vec{r}))]\right]\psi_i(\vec{r}) = \epsilon_i\psi_i(\vec{r}) \tag{8}$$

Here ϕ is the electron potential from the ions and the Hartree potential due to all the electrons, and $\mu_{xc}(\rho)$ is the local density approximation (LDA) potential due to exchange and correlation. The $N/2$ lowest eigenstates of this problem are used to generate the electronic density:

$$\rho(\vec{r}) = 2\sum_{i=1}^{N/2}|\psi_i(\vec{r})|^2 \tag{9}$$

where N is the number of electrons, and the factor of 2 is for spin. Since the potentials ϕ and μ_{xc} depend on ρ, the equations must be solved self-consistently. The total energy of the self-consistent solution is given by

$$E = \sum_i^N \epsilon_i - \frac{1}{2}\int\int\frac{\rho(\vec{r})\,\rho(\vec{r})}{|\vec{r}-r|}\,\mathrm{d}\vec{r}\,\mathrm{d}\vec{r} + \int\rho(\vec{r})\{\epsilon_{xc}(\rho(\vec{r})) - \mu_{xc}(\rho(\vec{r}))\}\,\mathrm{d}\vec{r} \tag{10}$$

Here $\epsilon_{xc}(\rho)$ is the exchange correlation energy in the local density approximation−approximate expressions for ϵ_{xc} and μ_{xc} exist in the literature.[29−31]

In conclusion of this section, we shall outline how typically the LDA is being used in practice in solid-state calculations. First one must specify the electron−ion interaction. This often is done within the framework of the pseudopotential theory,[32,33] or full potential calculations may be performed.[34] In pseudopotential theory the electrons of an atom are divided into two groups−the tightly bound core electrons and the valence electrons in the outer shells participating in the bond formation. Electrons in the first group are effectively excluded from the picture, by introducing the repulsive "orthogonalization" potential, which cancels most of the core potential seen by the outer shell. The result is a weak *pseudopotential* for the valence electrons. The technique has its roots in the orthogonalized plane wave (OPW) method. Most modern pseudopotential calculations use a variant of the norm conserving pseudopotential introduced by Hamann, et al.[35] For an overview of the earliest version of pseudopotential theory we would recommend an article by Cohen and Heine.[36] Once we have constructed the single-particle Hamiltonian, a basis set of functions is needed to solve the Schrödinger equation. One possible choice of a basis is a Fourier series known as plane waves. This program was realized by Ihm et al., who developed a momentum-space formalism for the total energy of solids.[37] Their formalism was designed particularly for applications with the self-consistent pseudopotential method. The appealing features of this method are the relative computational simplicity, and the fact that the basis set is unbiased, since no a priori assumptions about the shape of the wave-function have been made. The latest overview of the plane wave method can be found in ref 38. Local basis functions can also be used. In recent years, forces on atoms have been obtained by differentiating eq 10 with respect to atomic coordinates.

This allows simulation of motion of the atom and is generally referred to as quantum molecular dynamics. The dynamics is classical in that Newton's laws of motion for the nuclei are used but the forces are computed within a quantum mechanical framework for the electrons.

B. Quantum Molecular Dynamics of Interacting Fragments. The plane-wave total energy method based on the local density approximation to density functional theory and the pseudopotential technique has proven to be quite successful when applied to a variety of solids. The computational efficiency of this method has been significantly improved in the past decade, starting with the work of Car and Parrinello.[39] Although the new developments have made possible the study of systems containing a number of atoms of roughly an order of magnitude larger than before, the method is still computationally very demanding both in CPU time and memory requirements.

In 1989 Sankey and Niklewsky (SN)[40] introduced the ab initio multicenter tight-binding molecular dynamics method for covalent systems. The method takes advantage of the LDA energy functional discussed in the previous section. The salient feature of the technique is its extreme computational efficiency, which allows one to perform rapidly first-principles molecular dynamics simulations of large systems. In this method individual atoms are treated as Harris[41] fragments, and the whole solid forms the coupled system. In its later version,[42] the charge density is treated self-consistently allowing very ionic systems such as zeolites to be accurately modeled. The total energy is computed, and the quantum-mechanical forces acting on each atom are evaluated. A step of classical molecular dynamics is performed by solving the equations of motion. Many of the same steps are involved in the Car−Parrinello technique.[39]

Another important step toward a fast and accurate total energy method consists of choosing an efficient basis set for the determination of the occupied eigenvalues and eigenvectors of the one-particle Schrödinger equation. Sankey and Niklewski[40] have introduced the nonorthogonal "fireball" basis of pseudoatomic orbitals (PAO), which are obtained by solving the atomic problem with the boundary condition that the "atomic" orbitals vanish outside a predetermined radius R_c. Thus the energy eigenstate is a linear combination of PAOs:

$$\langle \vec{r} | \psi_i \rangle = \sum_{l,\mu} a_i(l) \phi_\mu^{\mathrm{PAO}}(\vec{r} - \vec{r}_l), \qquad (\mu = s, p) \quad (11)$$

where each PAO satisfies the Schrödinger equation for a free atom in the pseudopotential and LDA approximations but with the boundary condition

$$\phi^{\mathrm{PAO}}(\vec{r})|_{r_c} = 0 \quad (12)$$

An important advantage of this basis set is that the Hamiltonian (and overlap) matrix elements have a short range, which makes the matrix sparse. Also, the number of nonzero Hamiltonian matrix elements scales linearly with the size of the system.

All matrix elements are evaluated in real space. For the exchange-correlation matrix elements an elegant linearization was suggested. In addition, the integrals involving four-centers are not required,[42] so that all the two- and three-center integrals are readily tabulated beforehand and placed on interpolation grids no larger than two-dimensional.

The forces acting on each atom are determined by taking the derivative of the total energy with the respect to the atomic position:

$$\vec{F}_l = -\partial E_{\mathrm{tot}} / \partial \vec{R}_l \quad (13)$$

It should be noticed that in taking the necessary derivatives, derivatives are taken of the matrix elements, in contrast to taking the matrix elements of derivatives, so that Pulay corrections[43] are automatically and exactly included. The molecular dynamics simulations are performed by looking up the necessary matrix elements and their derivatives from the interpolation grids. The equations of motion are integrated using the Gear or Verlet algorithms.[18] Classical molecular dynamics simulations including the forces computed from quantum calculations of the electrons are referred to as quantum molecular dynamics, or QMD, simulations. The Sankey−Niklewski method has proven to be a very efficient and successful tool for a great variety of problems, including small clusters, bulk materials, and surfaces,[44] and the electronic structure of zeolites.[45] In the following two sections we shall use it to study the energetics of doping of zeolites and zeolite-like materials.

The Car−Parrinello plane-wave technique[39] is less approximate, but with a computation price. Other simplified QMD techniques also exist, and one used often for large systems is empirical tight-binding (ETB).[46−49] In this theory the following approximation to eq 10 is used. Matrix elements of the single-particle Hamiltonian in a nonspecified local basis between the orbitals $\phi_\mu(\vec{r} - \vec{R}_i)$ and $\phi_\nu(\vec{r} - \vec{R}_j)$ centered on atoms at $\vec{R}_i$ and $\vec{R}_j$, respectively, are approximated by analytic functions of the interatomic distance $H_{\mu\nu}^{\{\lambda\}}(|\vec{R}_i - \vec{R}_j|)$. Here $\{\lambda\}$ represents a set of fitting parameters. These functions are fit to reproduce the electronic band structure known either from the experiment or from ab initio calculations. The method is fast but has the main drawback of all empirical techniques: parameters of the model are not transferable and must be fitted for each problem individually. Progress in this direction has been limited primarily to Si an C semiconducting systems.

C. Order *N* Methods. The time-limiting factor of most current electronic structure methods is the $O(N^3)$ scaling due to diagonalization of the single particle Hamiltonian matrix, where N is the number of electrons in a supercell. This means that when you double the system size, the computational time increases eight times! Recently, several techniques were introduced, which in principle allow this bottleneck to be curcumvented by offering an $O(N)$ scaling.

These methods can be divided into two major categories: statistical methods and variational methods. Statistical methods use staistical or information theory approaches and have no obvious connection to the underlying physical problem they are meant to solve, and the linear scaling comes from the mathematics. Variational methods use an energy functional which is mininmized with respect to some degrees of freedom representing the electronic ground state, and the linear

scaling comes from the localized nature of the underlying quantum interactions in the system.

Let us start with a brief description of two statistical techniques. Drabold and Sankey[50] introduced a maximum entropy approach using importance sampling to compute the total density of states (DOS), band-structure energy (BSE) integrals, and related quantities. To determine the DOS and BSE, one actually does not need to know all the information contained in the wave function, but rather the "average" information contained in the diagonal matrix elements. The DOS $\rho(E)$, and particularly the BSE, are obtained by integrating $E \times \rho(E)$ up to the Fermi level. All the information carried by the density of states is contained in any one single vector ξ in the family of vectors of the form

$$\xi = \sum_{j=1}^{N} e^{i\phi_j}\psi_j/\sqrt{N} \tag{14}$$

where ϕ_j specifies an arbitrary phase, and ψ_j are the energy eigenstates. The expectation value of the DOS operator $\hat{\rho}(E) = \delta(E - \hat{H})$ between any ξ gives the exact density of states; $\rho(E) = \langle\xi|\hat{\rho}(E)|\xi\rangle$. The vectors ξ equally weigh all of the eigenvalues of the spectrum of H. For this reason such ξ vectors are called *impartial vectors*. The Hamiltonian H has moments μ_n

$$\mu_n = \int_{-\infty}^{\infty} dE\ E^n\rho(E) = (1/N)\ \mathrm{Tr}\ H^n \tag{15}$$

As can be seen an impartial vector also generates exact moments through its expectation value

$$\mu_n = \langle\xi|H^n|\xi\rangle \tag{16}$$

The point is that for a sparce Hamiltonian matrix (as in a local orbital technique), the expectation value is an $O(N)$ operation, while taking the trace in eq 15 is not. There are two key steps in the method. The first step is to effectively approximate ξ in some manner. This is done by selecting an appropriate random vector x and using a penalty function method to find an improved vector x^* closer to an impartial vector. The second step involves transforming the information contained in ξ into $\rho(E)$ in an $O(N)$ way. This is accomplished by viewing $\rho(E)$ as a probability distribution and using the maximum entropy principle (Maxent) to determine the best estimate from partial information (a finite set of moments). The price paid for this dramatically increased efficiency is that exact values of individual eigenvalues are not computed, but rather an accurate, continuous representation of the electronic DOS is obtained. A different way of using moment expansions was employed by Wang.[51] This method uses Chebyshev moments calculated using completely random wave functions, the moments are then transformed to energy space. A "Fermi projection" technique is used to keep unoccupied states from contributing to the expectation value of the Hamiltoninan. A similar technique was also developed by Goedecker and Colombo.[52] Both statistical methods do much better in the calculations of the DOS and BSE than in determination of the forces which must be used in molecular dynamics simulations. This is a severe limitation of the impartial vector technique.

We now describe the essence of the variational $O(N)$ methods. In this we follow the recent discussion by Vanderbilt.[53] These methods can be considered as special cases of a general approach introduced by Hernandez and Gillan.[54] Instead of using the true one-particle real-space density matrix

$$\rho(r,r') = \sum_{n,k} \psi^*_{n,k}(r)\ \psi_{n,k}(r') \tag{17}$$

(here $\psi_{n,k}(r')$ are the Bloch functions) one introduces an ansatz, or a *trial* density matrix x

$$x(r,r') = \sum_{i,j}^{M} L_{i,j}\phi^*_i(r)\ \phi_j(r') \tag{18}$$

where both the "Wannier-like" functions $\phi_i(r)$ and the site matrix $L_{i,j}$ are spatially localized in the region defined by some cutoff radius. The "true" density matrix is idempotent ($\rho^2 = \rho$) and has eigenvalues equal to either 0 or 1. Since there is no reason why the trial density matrix should be idempotent, one uses the "McWeeney transformation"

$$\rho = 3x^2 - 2x^3 \tag{19}$$

which has a local maximum at the point $\rho(1) = 1$ and a local minimum at the point $\rho(0) = 0$. Then one writes the energy functional

$$\Omega = \mathrm{Tr}(\rho(H_{\mathrm{bare}} - \mu)) + E_{\mathrm{Hxc}}(n) \tag{20}$$

where H_{bare} contains the kinetic energy and the external potential (due to the ions), $n(r) = \rho(r,r)$ and $E_{\mathrm{Hxc}}(n)$ is the Hartree and exchange-correlation functional of the density. This energy functional is then minimized with respect to $L_{i,j}$ and/or $\phi_i(r)$.

Several different schemes of such a minimazation have been suggested. Mauri et al.[55] or Ordejon et al.[56] have used $L_{i,j} = \delta_{i,j}$ and M equal to the number of occupied orbitals. The energy functional is minimized with respect to the functions $\phi_i(r)$ which are not orthonormal originally but become nearly so at the solution. Kim et al.[57] used an identical technique only the number of states M was larger than the number of occupied orbitals and the chemical potential μ had to be adjusted to have the right number of electrons. Hierse and Stechel[58] used M equal to the number of occupied orbitals but varied both $L_{i,j}$ and $\phi_i(r)$. Li et al.,[59] Daw,[60] and Nunes and Vanderbilt[61] used the so-called density-matrix scheme which results in fixing $\phi_i(r)$ to tight-binding orbitals and varying the $L_{i,j}$. M is kept equal to the number of tight-binding basis functions. The most general case was considered by Hernandez and Gillan. They varied both $L_{i,j}$ and $\phi_i(r)$ and used M larger tham the number of occupied orbitals.

$O(N)$ techniques have already made possible calculations of extremly large systems[51,62] and will definitely become an important tool of computational material science. They are particularly powerful when applied to insulating systems including biological ones such as DNA,[62] since the orbitals in these systems are naturally localized. So far $O(N)$ techniques have not been applied to zeolites, where they appear to be most promising.

IV. Energetics of Doping

A. Si Clusters in Silica−Sodalite. To explore the possibility of creating new structures and materials

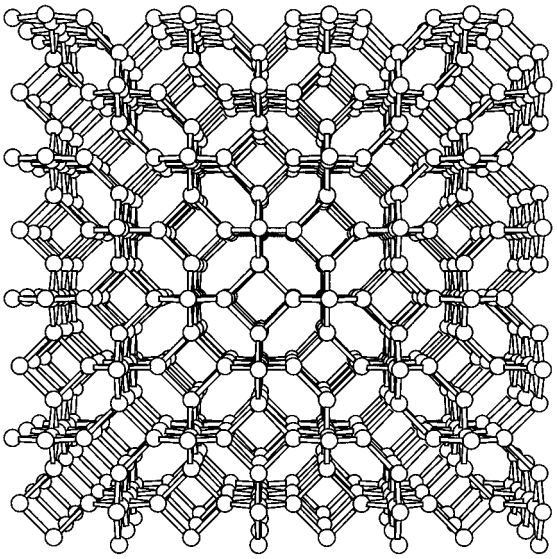

Figure 1. Sodalite lattice, where only the T atoms are shown.

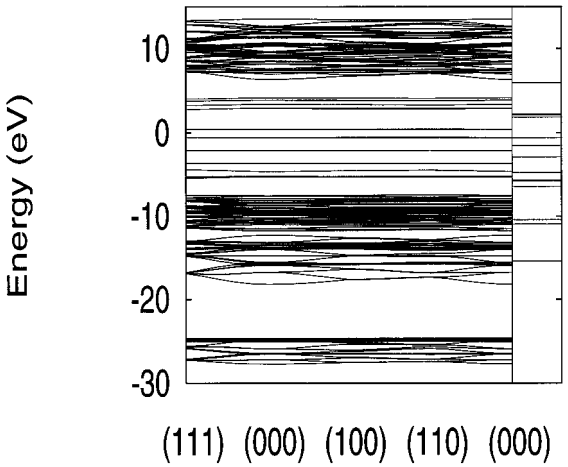

Figure 2. Band structure of Si_5 cluster inside the sodalite β-cage. For comparison, the levels of the Si_5 cluster in vacuum are shown in the right panel.

using zeolite frameworks we start with a simple "model" system—*Si* clusters in silica–sodalite. Silica–sodalite is the all-silicon version of the zeolite sodalite. Natural sodalite has a unit-cell composition $Na_4Al_3Si_3O_{12}Cl$, and its structure was unraveled by Pauling in 1930.[63] In 1985 Bibby and Dale reported the nonaqueous synthesis of a novel pure-silica form of sodalite,[64] which is Si_6O_{12}. The structure is shown in Figure 1. The unit-cell dimension was determined from the X-ray powder diffraction pattern to be 8.836 *Å*. They pointed out that unlike the rest of low-density silica polymorphs, silica–sodalite contains only six- and four-membered rings. The structure was refined in a later experiment of Richardson et al.[65]

There are several theoretical studies of silica–sodalite reported. Vibrational properties were studied both by the lattice dynamics method[66,67] and by molecular dynamics.[68] Studying supralattices of Si clusters is a good first choice to explore the physics of supralattices since the β-cage of sodalite is a structural element common to many zeolites, and there is a great deal of knowledge about small Si clusters.[69–71] However, there is nothing known experimentally about possible supralattices formed when the two are put together. For our purposes this system serves as a model.

We have studied the structure, electronic properties, and energetics of the clusters Si_2, Si_3, Si_4, Si_5, Si_6, and Si_7 in silica sodalite, since both silicon clusters and sodalite represent the simplest of both the cluster and zeolite systems. Full molecular dynamics relaxations were peformed using the self-consistent quantum molecular dynamics method known as Fireball-96.[42] Electronically, the doping forms bands in the middle of the SiO_2 bandgap which are very narrow due to the large separation of the guest species. An example is shown in Figure 2, the band structure of the supralattice of Si_5 clusters encapsulated inside the β cages of sodalite is compared with that of Si_5 clusters located on the body-centered cubic lattice of the same size. The dispersion in the case of the cluster is very small, so only the levels at the Γ point are shown in the right panel. The most striking result is that the electronic states of the cluster appear in the gap region of sodalite practically unchanged (there is, however, a slight upward shift in energy). A new composite material is predicted to have a bandgap equal to that of bulk silicon, but with hardly any dispersion of the band edges. Many-body correlations are known to be important for narrow bands, and further theoretical analysis will be needed, using a theory which explicitly deals with correlation effects, such a theory is described in section VII. The most surprising result that is found is that the electronic structure of *Si* clusters is not drastically altered by the cluster–host interaction. *This is contrasted with the case of alkali-metal atoms in sodalite (section VIA), where the electronic states of the cluster inside the zeolite are more similar to "cavity states" and are greatly influenced by the zeolite.* Since the Si cluster states are little altered by the zeolite, this suggests that one can form a new material with the electronic gap of the cluster—e.g., silica–sodalite "doped" with Si_5 is a direct bandgap material with a bandgap of bulk silicon. Si_7 inside silica–sodalite would result in a material with a bandgap in the highly desirable 2 eV region, although such a large cluster is energetically unfavorable in sodalite (see below).

The structure of the Si clusters inside the cages of silica–sodalite closely resembles that of the clusters in free space. There are some differences, however; for example, Si_4 in sodalite prefers the tetrahedron rather than rhombus in the ground state. When we look into energetics of these clusters we find that only the Si_n clusters with $n < 5$ have negative energies of encapsulation. The energy of encapsulation E_{enc} is defined in the following way: $nE_{enc} = E(\mathrm{Si}_n + \text{sodalite}) - E(\mathrm{Si}_n) - E(\text{sodalite})$ and measures the cost of cluster encapsulation per atom. This result is shown in Figure 3 and may be understood using the following argument. The volume of the β-cage is approximately 114 $Å^3$, while the volume per atom in the diamond phase of *Si* is 20.2 $Å^3$. Obviously a *Si* cluster is "squeezed" when Si_6 or Si_7 is put inside the cage.

In conclusion, we find that doping of zeolite cages with electronically active species allows creation of new electronic materials with pre-designed electronic properties. Silicon clusters are found to be weakly interacting with the host, and a number of molecular-like flat bands are formed in the sodalite bandgap. The silicon clusters/silica–sodalite is a "model" semiconductor cluster–zeolite system. The structure of the sufficiently

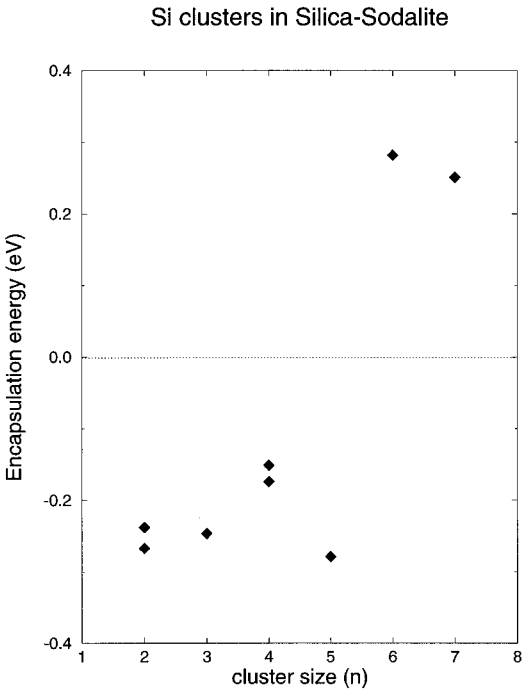

Figure 3. Energy of encapsulation for Si clusters in silica−sodalite.

small clusters (Si_n clusters with $n < 5$) is similar to that of clusters in free space.

B. Na-Doped Si Clathrates. A particularly simple example of a supralattice is alkali-metal-doped Si clathrates. It is particularly simple because the cluster inside the clathrate cage is a single alkali-metal dopant atom. Si compounds with the clathrate structure were first synthesized in 1965.[72] In the Si clathrates, metal impurity atoms, such as Na or K, stabilize the structure against collapse into a dense structure (in this case into the silicon diamond structure), just as the guest molecules do in the hydrate structures[72−75] or in zeolites. Both stoichiometric phases $NaSi_6$ and nonstoichiometric phases Na_xSi ($0 \leq x \leq 0.08$) are formed. Clathrate structures involving Ge with K impurities have also been prepared. It has been found that very low concentrations of metal atoms can be achieved, and with specific material processing, it should be possible that the metal atoms can be entirely removed. The same structures of Si clathrates, but made of SiO_2 with Si−O−Si bonds, replacing Si−Si bonds, have also been characterized as polymorphs of SiO_2 known as clathrasils, such as in naturally occurring melanophlogite from Mount Hamilton, CA.

Here, we examine the Si_{136} clathrate which has a lattice structure that is face centered cubic (fcc). Experimentally the Si bond length is near 2.37 *Å*, which is only slightly expanded compared to 2.35 *Å* for Si in the diamond structure; but due to cages within the structure, the volume per atom is expanded approximaely 18%. The bond lengths are not found to be sensitive to the concentration of metal atoms. The structure is derived from packing pentagonal dodecahedra (a small 20 atom fullerene-like cage) and hexakaidecahedra (a larger 28 atom cage) in the ratio 2:1, and the average ring size is 5.064 (the smallest of any known such structure). The dodecahedra (16 per unit cell) form intersecting face-sharing rods along ⟨100⟩ and the hexakaidecahedra (eight per unit cell) are in the

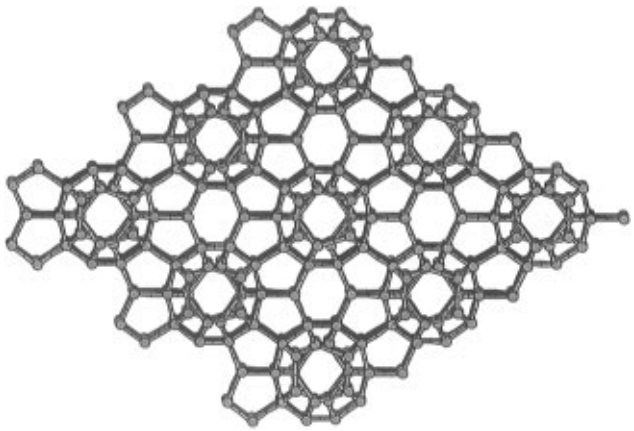

Figure 4. Projection of the Si_{34} clathrate lattice.

interstices of the packing. There are $4 \times 34 = 136$ Si atoms per cubic unit cell which has the same space symmetry as diamond. The high proportion of five-membered rings (ideal angle 108°) makes the structures energetically competitive with diamond (angle 109.5°). A projection of the structure is shown in Figure 4.

When alkali-metal atoms are present, we will use formulas of the type M_n @ Si_{136} to indicate that the cubic unit cell contains n metal M atoms (where M = Na, K, etc.) and 136 Si atoms. For example, Na_4Si_{136} means that there are four Na atoms in the cubic 136 atom cell. In contrast with alkali-metal-doped fullerenes where the dopant atoms are interstitial outside the polyhedra, in silicon clathrates they occupy interstitials within the polyhedra. Experimentally, the magnetic susceptibility disappears in Na_xSi_{136} when x reaches approximately 8, probably due to a transition from an insulator to a metal.[76] This composition is interpreted to be the composition in which every hexakaidecahedron is fully occupied. At lower Na concentrations the EPR measurements indicate the presence of well-separated Na atoms, and allow tracking of electron delocalization with increasing Na concentration. The first qualitative description of the insulator-to-metal transition in Si clathrates was given by Mott[77] in his interpretation of earlier experiments by Cros et al.[74]

We now discuss the energetics of the alkali-metal doping. We desire to know if there is a particular order, in which the large and small cages of Si_{136} are being occupied by Na atoms. The $Fd3m$ space group has 8 (b) sites within large cages and 16 (c) sites within small cages. We consider the following configurations. Configuration I ($Na_4^{8(b)}$@Si_{136}) half occupies the large cages with four Na atoms at the 8(b) sites, while configuration II ($Na_8^{8(b)}$@Si_{136}) fully loads the large cages with eight Na atoms at the 8(b) sites. In configuration III ($Na_4^{16(c)}$@Si_{136}), the small cages are one-quarter occupied by placing four Na atoms in each cell at 16(c) sites, and in configuration IV ($Na_8^{16(c)}$@Si_{136}) the small cages are one-half occupied by placing eight Na atoms in each cell at the 16(c) sites. Finally in configuration V ($Na_4^{16(c)}Na_4^{8(b)}$@Si_{136}), eight Na atoms in each cell are split into four occupying the large cages (half occupancy of 8(b) sites) and four occupying the small cages (one-quarter occupancy of 16(c) sites). This choice of configurations enables us to consider relatively isolated defects (distant pairs) and closely connected clusters (close pairs) in the regime of low-to-intermediate levels

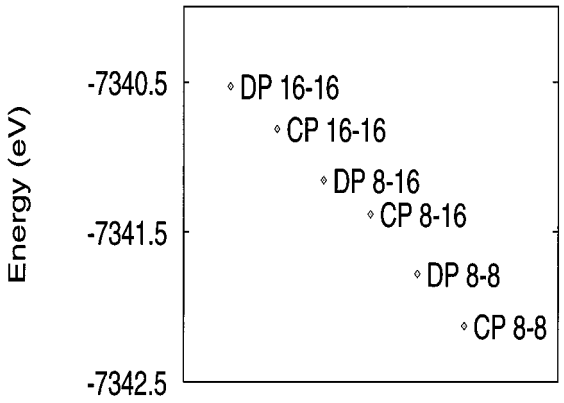

Figure 5. Energies for different configurations of Na in Si clathrate. DP and CP stands for "distant pair" and "close pair", respectively (see text). The occupation of a large cage at site 8(b) (in $Fd3m$) is denoted by 8, and of a small cage at site 16(c) by 16.

of doping. By comparing calculations with the same number of Na and Si atoms, we can directly obtain energy costs associated with occupying different sites. Quantum molecular dynamics is used to find the zero force geometry for each of these configurations. The results of these calculations are shown in Figure 5. We denote close pairs as CP, and separated (distant) pairs are denoted DP in the figure. For example, configuration IV is denoted CP 16−16 which stands for $Na_8^{16(c)}@Si_{136}$, and configuration III is denoted DP 16−16 which stands for $Na_4^{16(c)}@Si_{136}$. As can be seen, the close pair $Na_8^{8(b)}@Si_{136}$ has the lowest energy, which is lower than that of a distant pair by 0.35 eV/pair. This implies that under equilibrium conditions, large cages would be occupied first. After all large cages are occupied, then the small cages begin to be occupied. However, in this description, only the energy is considered and kinetic/entropic effects are neglected.

We have also investigated the electronic states for these system, and the details will be reported in a separate publication. The results of this investigation seem to suggest the following scenario for the metal-to-insulator transition in the Na-doped clathrate Si_{136}. At the low level of doping, only the large cages centered at 8(b) points are occupied with Na atoms. This results in a very narrow half-filled band near the conduction band edge of the pure material, which according to a single-electron theory should lead to a metallic material. However, many-body correlation effects likely cause the system to become an insulator via the Mott transition[78] (see section VII). When all of the large cages are occupied, the system becomes a narrow-gap semiconductor. As the doping level is increased, the small cages centered at 16(c) points become occupied. The highest occupied bands for these sites appear to have a large free-electron-like component due to the increased hopping interaction between the guest Na and Si framework. This results in electronic delocalization and metallic behavior. This qualitative picture is in agreement with the experiments of Roy et al.[76] They reported a correlation between the metal-to-insulator transition observed in the measurements of the magnetic susceptibility and relative occupancies of the 16(c) and 8(b) sites estimated from X-ray diffraction line intensities. The transition is observed when a noticable fraction of the 16(c) sites begin to be occupied. Obviously, more experiments are needed to fully document experimentally the different stages of the system's evolution, and the nature of the electronic states at each stage. These materials may find applied uses as high thermopower materials, or as novel correlated electron systems including superconductivity. Recently, it has been reported that Ba-doped Si clathrates are in fact superconducting.[79]

V. Cluster Formation

Partially, the original interest in what we now call supralattices came from the idea of using the zeolite framework as an assembler of nanosize particles to be used as quantum dot structures. For a specific guest in a chosen host framework, it is important to know the preferred arrangements of the ions within the framework cages and their electronic levels. Experimental information is often very difficult to obtain or interpret due to the complexity of the systems involved. The use of ab initio computer simulations may help with data interpretation, and in the interpolation to regimes unaccessible by experiments. We now review one such set of calculations to determine the geometry of sodium in zeolite Y.

A. Sodium-Doped Zeolite Y. Zeolite Y is a diamond arrangement of sodalite β-cages connected via hexagonal prisms. Alternatively, the structure may be described as a diamond lattice of large supercages connected by 12-membered rings. Each supercage shares 6-membered rings with four neighboring β-cages in a tetrahedral fashion. Essentialy, the structure of zeolite Y is that of the rare mineral faujasite with a high Si:Al ratio. Another related zeolite is zeolite X which has the same structure but a lower Si:Al ratio. The tetrahedral sites of zeolite Y are occupied by Al and Si connected by oxygens. Na counterions are present in the structure to compensate the charge deficiency caused by the substitution of Si by Al. There are natural lodging sites for these countercations in the structure, four of which are I, II, I′, and III. The site in the center of the hexagonal prism is labeled I. The site in the center of the hexagonal window shared by a supercage and a β-cage (on the supercage side) is labeled II. The site in the center of the hexagonal window shared by two sodalite cages is labeled I′. Because of the diamond symmetry there are four sites II per supercage and four sites I′ per sodalite cage. Cations may bind to any of the oxygen atoms on the 12-membered rings connecting supercages, and these sites are labeled III. Upon exposure of sodium zeolite Y (Na-Y) to low levels of sodium vapor causes this material to change its color from white to pink. This has been connected by the ESR experiments to formation of a Na_4^{3+} cluster. However, ESR experiments do not give us the complete picture. First, the location of such a cluster in the zeolite cannot be established, and thus it is difficult to determine which factors control the stability and formation of different clusters. Second, it is not clear whether all Na species are ESR active—there may be other species in the cages which are nonparamagnetic and thus "invisible" in the ESR experiment.

Ursenbach et al. have recently examined this problem theoretically.[80] As the "native" zeolite stoichiometry they chose $Na_{64}Si_{128}Al_{64}O_{384}$. In the conventional cubic cell there are eight sodalite β-cages and eight supercages

in the cell. Cages of both types contain four Na^+ ions, that adds up to 64 "native" countercations per conventional cell. To reduce computational effort, one chooses to use the primitive cell of the diamond lattice (fcc) so that the number of atoms may be reduced by a factor of 4, and only two supercages and two sodalite cages are contained in this primitive cell.

An attempt was made to use a parallel version of the Cambridge serial total energy package (CASTEP) known as CETEP (Cambridge-Edinburgh total energy package). It is a rather accurate density functional total energy method using pseudopotentials, periodic boundary conditions, and a plane-wave expansion for electronic wave functions. However, even the use of the modern parallel architecture was not nearly enough to use the plane-wave-based ab initio molecular dynamics for this system. The large size of the unit cell, exacerbated by the presence by the strong pseudopotential of oxygen (which requires a very large number of plane waves in the expansion), made the use of this method totally impossible.

To overcome this problem, Ursenbach et al. introduced an approximate technique which is a hybrid of the ab initio quantum mechanical description with an empirical classical potential. Two major assumptions were made. First, the quantum mechanical consideration was limited only to the electrons contributed by the alakli metal atom—the "native" zeolite structure was regarded as composed of Si^{4+}, Al^{3+}, O^{2-}, and Na^+ ions. Thus the problem is reduced to a few electrons in the external potential of the framework ions, which are assumed to have their formal charges. Secondly, the positions of the framework ions were held fixed, and the motion of Na^+ ions was described via classical potentials.

To better describe the interaction of the excess electrons with the framework oxygen ions, an approximate oxygen pseudopotential was introduced of the form

$$V_{eO^{2-}}(r) = \frac{q_e q_{O^{2-}}}{r}\,\mathrm{erf}(2r) + P(r) \tag{21}$$

where

$$P(r) = \begin{cases} 60 + 25.2525r^2 - 45.4963r^4 + 12.9014r^6 & r < 2.2\ \text{Å} \\ 0 & r > 2.2\ \text{Å} \end{cases} \tag{22}$$

The authors emphasized the importance of the short-range repulsive term $P(r)$. The parameters for the oxygen pseudopotential were fitted to reproduce the formation of the experimentally observed cluster Na_4^{3+}. The interaction of the electrons with cations was described using conventional ab initio pseudopotentials. A fairly low cutoff energy of 100 eV (dictated by the Na psedopotential) was used, which resulted in an expansion of the wave function that required ~32 000 plane waves per band. If the full peudopotential of oxygen had been used (which requires an energy cutoff of ~800 eV), roughly 725 000 plane waves would have been needed, which is nearly an unimaginable calculation. Due to the large size of the cell, only the Γ point was used to sample the Brillouin zone.

Essentially, the model just described treats the alkali cluster in the external potential of the zeolite framework, rather than the entire doped zeolite system. The assumption is made that the electronic energy levels available to the added electrons are much higher in energy than the valence levels of the host zeolite framework. Using this "rigid band" model for the framework means that effects of the electronic polarization are neglected.

The approximation of the immobile framework is also quite significant. Only the Na^+ ions were allowed to alter their positions. Empirical classical potentials of the Born–Mayer form due to Jackson and Catlow[81] were used for the interaction of the Na^+ ions with the Si^{4+}, Al^{3+}, and O^{2-} ions and are of the form

$$u(r_{ij}) = A_{ij}e^{-\rho_{ij}(r_{ij})} - \frac{C_{ij}}{r_{ij}^6} + \frac{Q_iQ_j}{r_{ij}} \tag{23}$$

where

$$A_{Na^+-O^{2-}} = 1226.84\ \text{eV}$$

$$\rho_{Na^+-O^{2-}} = 0.3065\ \text{Å}$$

$$C_{Na^+-O^{2-}} = 2.74\ \text{eV Å}^6 \tag{24}$$

Since the atoms of the zeolite were not allowed to move and react to the presence of the alkali atoms, the framework could not adopt configurations with more favorable binding sites.

Although Ursenbach et al. refer to their method as ab initio, one can see that it is in fact quite empirical. This underscores how difficult these systems are and how wide open for theory this field is. Taking into account these facts, this calculation represents a reasonable hybrid of ab initio and empirical methods—the ab initio portion deals with what seems to be the most important element of the system, while the empirical portion deals with the less important aspects.

We now review some of the results obtained from this modeling. Ursenbach et al. studied both the low doping and the high doping levels, the interactions of guest clusters in different sodalite cages, and large clusters in supercages. In this review we shall focus mainly on their results for the low doping limit.

We first consider the case of a single Na atom added to the supercage in each unit cell to form a supercell. Recall that there are 64 native sodium ions in the conventional cell, so that this doped configuration is denoted Na_1/Na_{64}-Y.

The Na ions are of two types, active and passive. The 64 passive Na ions are native (compensating Al) and are treated with empirical potentials and have no explicit electrons. The extra added Na ion is active in that its electron is explicitly included. Thus the quantum mechanical portion of the calculaton of the Na_1/Na_{64}-Y is that of a single electron in a very large conventional unit cell. The passive Na ions in the large supercage are not allowed to move except for the passive Na ions (arranged in a Na_4 cluster) in the small sodalite β-cage which are allowed to move. A single active Na atom is placed in the supercage. This is done after the few native Na ions, which are allowed to move, have been equilibrated during a short molecular dynamics

run at 300 K. To find the ground-state configuration, the active Na atom was moved around the supercage, and this motion was coupled to an A-type distortion of the Na_4 cluster in an adjacent sodalite β-cage. The minimum-energy configuration was found with the active Na^+ ion at the site III of the square window of the supercage, and the passive Na_4 cluster significantly contracted. The distance from the passive Na to the center of the sodalite cage reduced from the native zeolite value of 2.6 to 2.4 Å. Surprisingly, the single active electron was transferred from the supercage containing the active Na ion to the sodalite cage containing the passive Na_4 cluster. The energy of formation of −0.4 eV with respect to an empty zeolite cage and an isolated atom was found. However, such a comparison is not entirely consistent because the atom and the zeolite are calculated within different theoretical frameworks. The final configuration is reminescent of a small polaron. The large relaxation accompanying the formation of the Na_4^{3+} ion results in a high activation barrier (of the order of $^1/_2$ eV) for electron hopping from one sodalite cage to another.

An attempt was made that failed to stabilize a molecular-ion cluster in the supercage by bringing the active Na ion in proximity with the passive Na ions in the supercage. All supercage clusters were typically more than 1 eV higher in energy than the sodalite cage small polaron. This leads to the important conclusion that molecular ions at low levels of doping form only inside the sodalite cages. The stability of other clusters in the large supercage was also tested. Na_2, Na_3, Na_5, and Na_6 clusters were studied and found to be unstable.

Because the sodalite cages are well separated from each other, it was expected that adding more active Na inside the supercage would result in the formation of Na_4^{3+} small polaron molecular ions in other vacant sodalite cages. This was confirmed for the doping range from Na_1/Na_{64}-Y to Na_7/Na_{64}-Y. The border case appeared to be Na_8/Na_{64}-Y; starting from this stoichiometry, the extra electrons are forced into the supercage because all the sodalite cages become saturated.

Electrons localized on the small polaron sodalite Na_4^{3+} clusters weakly interact with each other. In such a system effects of electron correlation may be important. Uresenbach et al. discussed the effects of these interactions in the context of a Hubbard model (see section VII). Because of the strong autolocalization of an electron on the Na_4^{3+} cluster, they discounted hopping of an electron to an empty neighboring sodalite cage. To estimate the Hubbard parameters, they first calculated the energy of Na_2/Na_{64}-Y with two small polaron Na_4^{3+} clusters being nearest and next-nearest neighbors and found the energies of these configurations with respect to the native zeolite plus two free atoms to be −1.5 and −2.36 eV, respectively. Thus there is a tendency to prefer next-nearest neighbor configuration. Next, both electrons were put (with opposite spins) into a single sodalite Na_4 cluster. The difference between the two results suggests a Hubbard $U \sim 6$ eV. For the nearest-neighbor hopping matrix element $|T_{nn}|$ the value of 0.0014 eV was found, and for the next-nearest neighbor hopping $|T_{nnn}|$ that of 0.000 29 eV. The hopping integrals appear to be too small (even neglecting the polaron effect) to delocalize the electron over several sites at the low doping level. In this case the Hubbard model may be reduced to a Heisenberg exchange Hamiltonian with the exchange integral J_{ij} given by $|T_{ij}|^2/U$. For the nearest neighbors it gives $J_{nn} = 1.3 \times 10^{-6}$ eV, and for next-nearest neighbors $J_{nnn} = 6 \times 10^{-8}$ eV. This nearest-neighbor interaction J_{nn} corresponds to electron exchange on a time scale of ∼1 ns which is much shorter than the time scale of the ESR experiment (10 ns). Uresenbach et al. conclude that electrons associated with neighboring sodalite cages are being exposed to the nuclear fields in several cages on the time scale of the experiment, and hyperfine structure may not be resolved. Because the next-nearest neighbors are energetically preferred, exposure to several cages occurs when the sodalite Na_4^{3+} clusters can no longer avoid each other because of stoichiometry, i.e., above Na_4/Na_{64}-Y. These results are consistent with the experiments of Anderson and Edwards, who reported the collapse of the ESR hyperfine structure starting at the doping levels as low as Na_3/Na_{64}-Y.[82]

VI. Optical Properties

A. Electron Solvation in Zeolites. Sodalite is a relatively small unit-cell zeolite that consists of identical cubooctahedra also known as β-cages, or Kelvin polyhedra (familiar to physicists as a first Brillouin zone of an fcc lattice). The lattice is simple cubic with the space group $P\bar{4}3n$. The centers of the β-cages are on a body-centered-cubic lattice. The Si and Al atoms are located at the cage vertexes and are connected by oxygen bridges. There are only 6- and 4-fold rings in the structure, and the number of Al atoms is equal to that of Si atoms in the ideal structure. The electron deficiency caused by the Al/Si substitution is compensated by the presence of Na^+ ions, and such so-called dry sodalite has a unit formula $Na_6[SiAlO_4]_6$. The unit cell consists of two β-cages with Na ions located near the centers of hexagonal faces. This material is a wide-bandgap insulator with the gap of approximately 6 eV.[10]

When exposed to Na vapor, dry sodalite changes colors from white to light blue (low doping limit), and with increasing Na concentration to blue, then purple, and finally black (high doping limit). Black sodalite has four Na ions in every cage, forming tetrahedra. Three of the Na electrons compensate the Al, while the fourth electron is "extra" and dopes the sample. This excess electron is said to be solvated in sodium−sodalite. The system is somewhat analogous to color centers in ionic crystals. We now discuss a simple theory that explains the optical absorption spectra of this system given that we know the atomic positions.

Haug et al. introduced a simple model to calculate the spectrum of the Na-doped sodalite in the low concentration limit (isolated Na_4 clusters).[83] They limited their consideration to the excess solvated electron. The zeolite framework is assumed to be rigid, and the framework atoms were treated as point charges. With these approximations they write the following Hamiltonian for the excess electron:

$$\hat{H} = (p^2/2m) + V(r;R,Q) \qquad (25)$$

where the first term is the kinetic energy of the electron, and the second term describes the interaction of the electron with the framework atoms. The electron position and momentum are **r** and **p**, respectively. The

positions of the framework atoms as well as the Na ions in the cluster are denoted by **R**, and their charges by **Q**. The electron ground state in configuration space, $\langle x,y,z|g\rangle$, was found using the imaginary time propagator method:

$$\langle x,y,z|g\rangle = \lim_{\beta\to\infty}\langle x,y,z|\exp(-\beta\hat{H})|\Psi\rangle \qquad (26)$$

where β is a real number with units of inverse energy. The idea is that starting from any state Ψ (which must not be orthogonal to the ground state), propagating in imaginary time to infinity dampens states according to their energy, and only the ground state will survive. This is trivially proven by expanding the state Ψ in a complete set of the eigenfunctions of the Hamiltonian. Another way to think of it is that the imaginary time operator $e^{-\beta\hat{H}}$ acts like the Gibbs probability factor, which as $\beta \to \infty$ corresponds to $T = 0$ K and therefore picks out only the ground state.

To calculate the absorption spectrum, they used time-dependent quantum mechanics. The following expression was used to calculate the absorption cross section:

$$\sigma(\omega;\tau) \sim \omega \ \mathrm{Re} \int_0^\infty \mathrm{d}t\, f_\tau(t) \exp(i\omega t) C(t) \qquad (27)$$

Here $C(t)$ is the overlap integral (proportional to the matrix element of the dipole interaction between the initial state and the state at the time t), and a "window" function $f_\tau(t)$ is introduced to compensate for the finite integration over the time domain:

$$f_\tau(t) = \exp[-(t/\tau)^2] \qquad (28)$$

The window function cuts off the time evolution beyond the time τ; thus a spectral resolution is introduced in the problem. The time τ is the time for the promoted state (the state excited by the dipole interacton with light) to explore the potential energy surface.

The interaction between the electron and the framework is described by two-body, spherically symmetric, energy-independent local potentials:

$$V(r;\{R,Q\}) = \sum_i -e^2 Q_i \exp[-(|r - R_i|/\lambda)^4]/\min((|r - R_i|, R_i^c) \qquad (29)$$

The sum is taken over the framework atoms and the Na cluster. The values of $\lambda = 15.0-25.0$ Å were used. R_i^c is a cutoff distance which truncates the Coulomb potential. Note that there are no true long-range Coulomb effects in this model.

The spectrum consists of approximately six peaks centered around 3 eV and spread over the range of approximately 1 eV. Haug et. al. have studied how the different parameters of the Hamiltonian in their model effect the resulting absorption spectrum:

(i) The dependence of the absorption spectrum on the framework charges. Five different sets of atomic charges were tried. It was known from ESR experiments that the excess electron is localized on the Na_4 cluster; that fact allowed one set to be immediately dismissed. The spectrum was found to be sensitive to the charges of the zeolite atoms only when the set with the ionic character close to 50%.

(ii) Time scales of the absorption spectrum and electron dynamics. Sampling time from 5 to 40 fs were tried. Results suggested photoconductivity in the low concentration limit.

(iii) The dependence of the absorption spectrum on the dimension of the Na_4 clusters. It was found that the increase of the cluster radius (the distance from the Na ion to the center of the cluster) by 0.3 Å causes an enormous red-shift of the spectrum by almost 2 eV.

(iv) The dependence of the absorption spectrum on the orientation of the Na cluster was found to be significant.

(v) Polarization effects—the absorption spectrum was sensitive to the laser polarization.

(vi) Alkali substitution effects were mimicked by changing the cutoff distance R_c^i. Calculations for K, Na, and Li showed that the overall structure of the spectrum does not change significantly upon these substitutions.

Although these calculations were encouraging, without more complete experimental input it was impossible to choose the best set of parameters. In a subsequent paper, Srdanov et al. measured the absorption spectra in the low doping limit which provided the information necessary for the best parameter assignment.[84] The wide breadth of the spectra (1.5 eV) did not allow an investigation of the effects of cluster orientation, laser polarization or the sampling time for the excited state. However, the estimate of the atomic charges was made ($Q_{Si} < +2$, $Q_{Al} < +1$, $Q_O > -1$, and $Q_{Na} = +1$), and the Na atom-center cage distance was estimated to be 2.401 Å.

The model was later extended for the saturation (high doping) limit in the work of Monnier et al.[85] They performed electronic structure calculations using the empirical pseudopotential between the solvated electron and the framework and Na ions of the form

$$V(r) = -q\ \mathrm{erf}(r/R_c)/r \qquad (30)$$

The effective charges q_i were modified from those of Haug et al.,[83] and the imaginary time propagation method was again used. Monnier et al. calculated the band structure of the doped sodalite and found that the system is a narrow-band metal. For comparison, they also calculated the band structure of a periodic arrangement of Na tetrahedra on a body-centered-cubic lattice (identical with the arrangement of the β-cages of sodalite) but without the sodalite $AlSiO_4$ framework. They found that the lowest conduction bands of the saturated sodalite closely resemble the two lowest bands of the tetrahedral sodium. Thus the effect of the electron–framework interaction seemed to be to put these states into the bandgap of sodalite. The fact that the metallic band was narrow suggested that one should go beyond a one-electron model to investigate the possible effects of electron correlations.

Using the pseudopotential band structure calculation, Monnier et al. have fitted their results to an empirical tight-binding Hamiltonian, which was used to estimate the effect of electron–electron interactions. They estimate the Hubbard U (the Coulomb interaction energy between two electrons residing in the same β-cage) to be about 6.18 eV. In addition they found that the energy required to transfer an electron from one cage to another cage when it is already occupied by a different electron to be 4.4 eV. This energy is much larger than the hopping integral of their tight-binding model. On the basis of these facts, they suggested the

possibility of Mott localization. Mott localization is a metal-to-insulator transition which occurs when the electron hopping from one lattice site to another is impeded by a strong Coulomb repulsion from other electrons already residing on this site.

More recently a major refinement of the model has been performed by Blake et al.[86] The magnitude of the charge on the framework atoms was now provided by ab initio STO-3G calculations. The ion−frame interaction included a short-range Born−Mayer repulsion, as well as a dispersion and an induced dipole−monopole interaction. The long-range Coulomb interaction was calculated via the Ewald summation. In this work the positions of the Na^+ ions were optimized in the force field of the rigid framework. It was found that the radius of the Na tetrahedron is smaller by 0.32 *Å* for the doped dry sodalite than that given by the formal charge model. The adiabatic ground state was calculated using a third-order Lanczos method, and a 10-fold improvement in computational efficiency was achieved over the method previously used by Haug et al.[83] Time-dependent perturbation theory was used to calculate the optical absorption spectrum. One of the main conclusions of this work is that the problem is sensitive to the long-range part of the electron−framework potential. An important accomplishment of this work is that all parameters but one (the size of the oxygen charge) were determined prior to the calculation of the absorption spectrum.

In conclusion, we would like to emphasize that by saturating sodium sodalite with Na, a new material is created. Sodium metal is separated into small clusters supported by the zeolite frame. The resulting material has very little resemblance to other sodium compounds or sodium metal. By modifying chemically the framework, one can at least partially control the properties of the resulting nanocomposite.

VII. Many-Electron Effects

One material which appears to show magnetic effects and in which there have been several experiments is K clusters in Linde type A (LTA) zeolites. LTA is an expanded variant of the sodalite structure in which the cubooctahedra (the β-cage) of sodalite are separated and bonds are formed across the rectangular faces. Expanding the lattice in this way opens up large cavities between cubooctahedra called α-cages, or supercages. Each supercage with a diameter of approximately 11 *Å* is surrounded by eight sodalite β-cages. The lattice is simple cubic with an α-cage at each lattice point. The potassium ions are ion-exchanged into Na-LTA and the "charge balanced" material is $K_{12}Al_{12}Si_{12}O_{48}$.[87] Excess K^+ ions may also be incorporated, and it is these excess ions that donate electrons to the system, producing a drastic change in the optical spectra (the material changes from white to a dark brick red color), and to the magnetic properties. This is similar to the solvated electron in sodalite described in section VIA. The active K is incorporated into the supercages of LTA, and the excess doping can be varied, which varies the size of the K cluster.

The most intriguing aspect of the K-LTA system to fully understand is the ferromagnetic behavior observed at low temperature. The atomic species (K) is of course nonmagnetic. The ferromagnetism does not occur in lightly doped samples, only in highly doped material. This suggests that it is an electronic interaction between the clusters in one supercage and the cluster in a neighboring supercage that is responsible. Kodaira et al.[88] report ferromagnetism with $2-3 < n < 6-7$, where n is the average number of K 4s electrons in the cluster.

Clusters in zeolites offer a unique opportunity to study a true many-body correlated electron system. The number of electrons (band filling) is adjustable by altering the doping, and the parameters which determine the correlated ground state can be altered by using a different supercage, e.g., the supercage in faujasite and Linde type A have different sizes.

Modeling the ferromagnetic interactions is difficult since it results from electron correlations with the many-body system. Delocalized electrons, such as in K metal, exhibit Pauli paramagnetism or Landau diamagnetism. The K-LTA system studied by Nozue et al.[87−89] has aspects of both a localized and a delocalized system. The interactions must be modeled using a Hubbard Hamiltonain, and this was done by Chowdhury et al.[90] following the work of Nozue et al.[89]

Let us examine the physics and chemistry of this modeling. The α-cage is assumed to a first approximation to act as a spherical well for the electrons of the the K-cluster (this assumption is quite unlike the assumptions made in the modeling of Na doped zeolite Y[80] discussed section VA, where the excess electron resides in the smaller β-cages). The electronic state in each cage can tunnel to one of its six neighboring cages on the simple cubic lattice. Neglecting for the moment this tunneling, the energies for the lowest s-, p-, and d-states of a spherical well of radius "a" are $E_L = \hbar^2 k_L^2/2m$, where $k_L = \pi/a$, $1.43\pi/a$, and $1.83\pi/a$ for $L = 0$, 1, and 2, respectively, where L is the orbital angular momentum. For an α cage of radius 5.5 *Å* for LTA, we find $E_s = 1.24$ eV, $E_p = 2.54$ eV, and $E_d = 4.25$ eV. At low concentrations of K, only the lowest s-level is occupied, and dipole-allowed s-to-p transitions occur and are expected at 1.3 eV. Qualitatively, this is in reasonable agreement with the experimental optical absorption bands B_1 and B_2 at 1.22 and 1.0 eV respectively.[88] The fact that there are two peaks instead of one is believed to be due to the interaction of the wave function of one cage with one in a nearby cage (tunneling). It is remarkable that such a simple model seems to give a first-order interpretation of the results. Note that in this picture the physics is controlled not by the K ion but rather by the geometry of the cage itself. To test this further, Kodaira et al.[88] ion exchanged Rb to from Rb-LTA and found an absorption spectrum in the same energy range as for K-LTA. There was a slight difference in the shape of the absorption spectrum, however, but overall the results support the conclusion that the framework itself controls the absorption.

We now examine the high-density K-doped region which is the ferromagnetic region and which presents the greatest challenge to theory. Here the S state is fully occupied by two electrons and electrons begin to partially occupy the 6-fold degenerate (including spin) p state (T_{1u} in cubic symmetry).

Experimentally, the magnetization takes on its maximum value when the T_{1u} level is approximately half occupied with three electrons. Choudhury et al.[90] modeled this system with a Hubbard Hamiltonian,

which for a half-filled s-like level normally gives an antiferromagnetic or paramagnetic metal. The inclusion of p-like levels changes the behavior. The model many-body T_{1u} Hamiltonian is

$$H = -\sum_{l\sigma,l'\sigma',\lambda\lambda'} a^{\dagger}_{l\sigma}(\lambda)t_{ll'}(\lambda\lambda')a_{l\sigma}(\lambda') + U\sum_{l\lambda} n_{l\uparrow\lambda}n_{l\downarrow\lambda} - J\sum_{l\lambda\lambda'(\lambda\neq\lambda')} \vec{S}_{l\lambda}\cdot\vec{S}_{l\lambda'} \quad (31)$$

Here $a^{\dagger}_{l,\sigma}(\lambda)$ creates an electron at lattice site l, of spin σ ($\uparrow$ or $\downarrow$), on orbital λ (p_x, p_y, or p_z), and $n_{l\uparrow\lambda} = a^{\dagger}_{l,\uparrow}(\lambda)a_{l,\uparrow}(\lambda)$ is the number operator. The spin operator S is $^1/_2\sum_{\mu,\nu}a^{\dagger}_{l,\mu}(\lambda)\vec{\sigma}_{\mu\nu}a^{\dagger}_{l,\nu}(\lambda)$, where $\vec{\sigma}_{\mu\nu}$ are the μ, ν elements of the Pauli spin matrixes. For the z component $(S_{l,\lambda})_z = {}^1/_2(a^{\dagger}_{l,\uparrow}(\lambda)a_{l,\uparrow}(\lambda) - a^{\dagger}_{l,\downarrow}(\lambda)a_{l,\downarrow}(\lambda))$ which counts the difference in occupation of spin-up and spin-down electrons.

This model is a many-body model that attempts at the onset to include correlations between the electrons. The hopping matrix elements $t_{l,l'}(\lambda,\lambda')$ take into account the tunneling of an electron in one α-cage at l to another at l'. If these quantities t are very large, the electron will tend to delocalize itself and exist as a paramagnetic free electron-like metal. The quantity U is the electron−electron repulsive integral ($U > 0$) which correlates two electrons at a single site (one expects U to be large for small cages and vice versa). U tends to localize the electron since the electron−electron interaction is minimum when each electron is allowed to reside in its own cage segregated from other electrons. The term J ($J > 0$, but with an overall minus) is an exchange integral whose physics is to reduce the Coulomb repulsion between two electrons on two different p orbitals (e.g., p_x and p_y) if their spins are aligned. This physical phenomenon occurs because of the overall antisymmetry of the Fermion wave function (Pauli exchange principle) which tends to keep two like spins (symmetric spin part of the wave function) further away spatially from each other by making the spatial part of the wave function antisymmetric. Such modeling is approximate since one must first obtain the parameters t, U, and J and then solve the many-body Hamiltonian to determine the ground state. Finally, statistical mechanics may be used to find the temperature dependence of the system. There have been several theoretical papers dealing with obtaining the Hubbard model parameters using local density approximation techniques.[91−93] For the problem of LTA supercages, order of magnitude values for t (to nearest neighbors) and for $U + J$ are 0.1 and 1 eV, respectively.

Although an exact ground-state solution of eq 31 is extremely difficult to obtain, it can be solved simply, but approximately, using mean-field theory. Choudhury et al. find the ground state of the system to take on all three possible states (ferromagnetic, antiferromagnetic, and paramagnetic) as a function of the Hubbard parameters. This contrasts with the Hubbard model for a nondegenerate s-states which generally gives antiferromagnetic states or paramagnetic states only. The desired ferromagnetic state is "sandwiched" in parameter space between the antiferromagnetic state and paramagnetic state. Thus the model only shows that the observed ferromagnetic state can exist, but since the parameters must simply be chosen to give the experimental result, the conclusion that the model given by eq 31 "explains" the experiment is not conclusive. However, these calculations illustrate an important and somewhat unexpected point which is that the ferromagnetic state is stabilized substantially by second-neighbor interactions. The first neighbors are at sites $l_1 = a(100)$ and second neighbors are at sites $l_2 = a(110)$. Adding hopping integrals t_{0,l_2} changes the single particle energies $E_n(k)$ and causes the electronic density of states to form three peaks instead of one. This destroys the perfect nesting of the bands, which favors the antiferromagnetic state and tips the energetics to favor the ferromagnetic state. However, it is difficult to see in LTA why these second-neighbor interactions would be nonnegligible, and so this observation must be interpreted with caution.

VIII. Conclusions

Regular 3D arrays of nanosize clusters can be synthesized in the cages of zeolite frameworks. Such nanocomposites are known as supralattices. Zeolites already have many industrial applications, and supralattices appear to be a potential "futuristic" new use for them. The zeolite framework acts as templates for semiconductor or metal supralattices, whose electronic properties of the guest/framework can be quite novel. The large size and complexity of these systems make them a challenge to solid-state theorists. In this article we have tried to demonstrate that electronic structure based methods, although computationally demanding, are now able to address some of the important issues to obtain an understanding on a microscopic scale of the properties of these nanocomposites. Solid-state methods provide a unified framework for studying both reactivity and structure of zeolites. The field is wide open and enormously exciting. The tremendous advances in electronic structure theory and computing power now finally make these systems accessible.

Acknowledgment. We thank the NSF (DMR-9526274) and the Office of Naval Research (Grant ONR 00014-90-J-1304) and the NSF High Pressure Material Synthesis MRG (Grant DMR-9121570) for support. It is been our pleasure to benefit from conversations with Michael O'Keeffe, Paul McMillan, Omar Yaghi, James Lewis, Wolfgang Windl, Anthony K. Cheetham, Galen D. Stucky, Nick Blake, and Marie-Louise Saboungi that we had during the course of this work.

References

(1) Stucky, G. D.; Srdanov, V. I.; Harrison, W. T. A.; Gier, T. E.; Keder, N. L.; Moran, K. L.; Haug, K.; Metiu, H. In *Supramolecular Architecture*; Bein, T., Ed.; American Chemical Society, Washington, DC, 1992.
(2) Smith, J. V. *Chem. Rev.* **1988**, *88*, 149.
(3) Dyer, A. *Chem. Ind.* **1984**, 241.
(4) Bogomolov, V. N.; Lutsenko, E. L.; Petranovskii, V. P.; Kholodkevich, S. V. *JETP Lett.* **1976**, *23*, 483. Bogomolov, V. N.; Kholodkevich, S. V.; Romanov, S. G.; Agroskin, L. S. *Solid State Commun.* **1983**, *47*, 181.
(5) Wang, Y.; Herron, N. *J. Phys. Chem.* **1988**, *92*:4988.
(6) MacDougall, J. E.; Eckert, H.; Stucky, G. D.; Herron, N.; Wang, Y.; Moller, K.; Bein, T.; Cox, D. *J. Am. Chem. Soc.* **1989**, *111* 8006.
(7) Tamura, K.; Hosokawa, S.; Endo, H.; Yamasaki, S.; Oyanagi, H. *J. Phys. Soc. Jpn.* **1986**, *55*, 528.
(8) Katayama, Y.; Yao, M.; Ajiro, Y.; Inui, M.; Endo, H. *J. Phys. Soc. Jpn.* **1989**, *58*, 1811.

(9) Parise, J. B.; MacDougall, J. E.; Herron, N.; Farlee, R.; Sleight, A. W.; Wang, Y.; Bein, T.; Moller, K., Moroney, L. M. *Inorg. Chem.* **1988**, *27*, 221.
(10) Smeulders, J. B.; Hefni, M. A.; Klaassen, A. A. K.; de Boer, E.; Westphal, U.; Geismar, G. *Zeolites* **1987**, *7*, 347.
(11) Moller, K.; Bein, T.; Herron, N.; Mahler, W.; Wang, Y. *Inorg. Chem.* **1989**, *28*, 2914.
(12) Samant, M. G.; Boudart, M. *J. Phys. Chem.* **1991**, *95*, 4070.
(13) Blatter, F.; Blazey, R. W.; Portis, A. M. *Phys. Rev. B* **1991**, *44*, 2800.
(14) Sun, T.; Seff, K. *J. Phys. Chem.* **1993**, *97*, 5213.
(15) MacDougall, J. E.; Stuckey, G. D. In *On Clusters and Clustering, From Atoms to Fractals*; Reynolds, P. J., Ed.; Elsevier Science Publishers: Dordrecht, 1993, p 273. Stucky, G. D.; MacDougall, J. E. *Science* **1990**, *247*, 669.
(16) Ozin, G. A.; Kuperman, A.; Stein, A. *Angew. Chem., Int. Ed. Engl.* **1989**, *28*, 359.
(17) Born, M.; Oppenheimer, R. *Ann. Phys.* **1927**, *84*, 457.
(18) Allen, M. P.; Tildsley, D. J. *Computer Simulations of Liquids*; Clarendon Press: Oxford, 1992.
(19) Van Beest, B. W. H.; Kramer, G. J.; van Santen, R. A. *Phys. Rev. Lett.* **1990**, *64*, 1955.
(20) Tsuneyuki, S.; Tsukada, M.; Aoki, H.; Matsui, Y. *Phys. Rev. Lett.* **1988**, *61*, 869.
(21) Henson, N. J.; Cheetham, A. K.; Gale, J. D. *Chem. Mater.* **1994**, *6*, 1647.
(22) Catlow, C. R. A., Ed.; *Modelling of Structure and Reactivity in Zeolites*; Academic Press: London, 1992.
(23) Sauer, J. In *Zeolites and Related Microporous Materials: State of the art 1994*; Weitkamp, J.; Karge, H. G.; Pfeifer, H.; Hölerich, W., Eds.; *Stud. Surf. Sci. Catal.* **1994**, *84*, 2039.
(24) Lubos, M.; Martin, R. M. *Phys. Rev. Lett.* **1994**, *72*, 2438.
(25) Hohenberg, P.; Kohn, W. *Phys. Rev.* **1964**, *136*, B864.
(26) Kohn, W.; Sham, L. J. *Phys. Rev.* **1965**, *140*, A1133.
(27) Silvi, B. *J. Mol. Struct. (THEOCHEM)* **1991**, *226*, 129.
(28) Hess, A. C.; McCarthy, M. I.; McMillan, P. F. In *Advances in Molecular Electronic Structure Theory*; Dunning, T. H., Jr. Ed., JAI Press Inc.: London, 1994; Vol. 2, p 143.
(29) Ceperly, D. M.; Alder, G. J. *Phys. Rev. Lett.* **1980**, *45*, 566.
(30) Perdew, J.; Zunger, A. *Phys. Rev* **1981**, *23*, 5048.
(31) Becke, A. D. *Phys. Rev. A* **1988**, *38*, 3098. Becke, A. D. *J. Chem. Phys.* **1986**, *84*, 4524. Perdew, J. P.; Yue, W. *Phys. Rev. B* **1986**, *33*, 8800.
(32) Cohen, M. H.; Heine, V. *Phys. Rev.* **1961**, *122*, 1821.
(33) Cohen, M. L. *Phys. Today* **1979**, *32*, 40.
(34) Blaha, P.; Schwartz, K.; Sorantin, P.; Trickey, S. B. *Comput. Phys. Commun.* **1990**, *59*, 399.
(35) Hamann, D. R.; Schlüter, M.; Chiang, C. *Phys. Rev. Lett.* **1979**, *43*, 1494.
(36) Cohen, M. L.; Heine, V. *Solid State Phys.* **1970**, *24*, 37.
(37) Ihm, J.; Zunger, A.; Cohen, M. L. *J. Phys. C* **1979**, *12*, 4409.
(38) Payne, M. C.; Teter, M. P.; Allan, D. C.; Arias, T. A.; Joannopoulos, J. D. *Rev. Mod. Phys.* **1992**, *64*, 1045.
(39) Car, R.; Parinello, M. *Phys. Rev. Lett.* **1985**, *55*, 2471.
(40) Sankey, O. F.; Niklewski, D. J. *Phys. Rev. B* **1989**, *40*, 3979.
(41) Harris, J. *Phys. Rev. B* **1985**, *31*, 1770.
(42) Demkov, A. A.; Ortega, J.; Sankey, O. F.; Grumbach, M. P. *Phys. Rev B* **1995**, *52*, 1618.
(43) Pulay, P. *Theor. Chim. Acta* **1979**, *50*, 299.
(44) Adams, G. B.; Sankey, O. F.; Page, J. B.; O'Keeffe, M. *Science* **1992**, *256*, 1792. Demkov, A. A.; Sankey, O. F. *Phys. Rev. B* **1993**, *48*, 2207. Demkov, A. A.; Sankey, O. F.; Schmidt, K. E.; Adams, G. B.; O'Keeffe, M. *Phys. Rev. B* **1994**, *50*, 17001.
(45) Demkov, A. A.; Sankey, O. F.; In *Access in Nanoporous Materials*; Pinnavaia, T. J.; Thorpe, M. F. Eds.; Plenum Press: New York, 1995; p 273.
(46) Sankey, O. F.; Allen, R. E. *Phys. Rev. B* **1986**, *33*, 7164.
(47) Goodwin, L.; Skinner, A.; Pettifor, D. *Europhys. Lett.* **1989**, *9*, 701.
(48) Xu, C.; Wang, C.; Chan, C. T.; Ito, K. *J. Phys. Condensed Matter* **1992**, *4*, 6047.
(49) Menon, M.; Subbaswamy, K. R. *Phys. Rev. Lett.* **1991**, *67*, 3487. Menon, M.; Subbaswamy, K. R. *Phys. Rev. B* **1993**, *47*, 12754.
(50) Drabold, D. A.; Sankey, O. F. *Phys. Rev. Lett.* **1993**, *70*, 3631.
(51) Wang, L.-W. *Phys. Rev. B* **1994**, *49*, 10154.
(52) Goedecker, S.; Colombo, L. *Phys. Rev. Lett. 73* **1994**, 122.
(53) Vanderbilt, D. *SECAM Conference on O(N) methods*; Lyon, France, 1995, unpublished.
(54) Hernandez, H.; Gillan, M. J. *Phys. Rev. B* **1995**, *51*, 10157.
(55) Mauri, F.; Galli, G.; Car, R. *Phys. Rev. B* **1993**, *47*, 9973. Mauri, F.; Galli, G. *Phys. Rev. B* **1994**, *50*, 4316.
(56) Ordejon, P.; Drabold, D. A.; Grumbach, M. P.; Martin, R. *Phys. Rev. B* **1993**, *48*, 14646.
(57) Kim, J.; Mauri, F.; Galli, G. *Phys. Rev. B* **1995**, *52*, 1640.
(58) Hierse, W.; Stechel, E. B. *Phys. Rev. B* **1994**, *50*, 1781.
(59) Li, X.-P.; Nunes, R. W.; Vanderbilt, D. *Phys. Rev. B* **1993**, *47*, 10891.
(60) Daw, M. *Phys. Rev. B* **1993**, *47*, 10895.
(61) Nunes, R. W.; Vanderbilt, D. *Phys. Rev. B* **1994**, *50*, 17611.
(62) Lewis, J. P.; Ordejon, P.; Sankey, O. F.; *Phys. Rev. Lett.*, submitted.
(63) Pauling, L. *Z. Kristallogr.* **1930**, *74*, 213.
(64) Bibby, D. M.; Dale, M. P. *Nature* **1985**, *317*, 157.
(65) Richardson, J. W.; Pluth, J. J.; Smith, J. V.; Dytrich, W. J.; Bibby, D. M. *J. Phys. Chem.* **1988**, *92*, 243.
(66) Nicholas, J. B.; Hopfinger, A. J.; Trouw, F. R.; Iton, L. E. *J. Am. Chem. Soc.* **1991**, *113*, 4792.
(67) De Man, A. J. M.; van Beest, B. W. H.; Leslie, M.; van Santen, R. A. *J. Phys. Chem.* **1990**, *94*, 2524.
(68) Smirnov, K. S.; Bougeard, D. *J. Phys. Chem.* **1993**, *97*, 9434.
(69) Sankey, O. F.; Niklewski, D. J.; Drabold, D. A.; Dow, J. D. *Phys. Rev. B* **1990**, *41*, 12750.
(70) Ragavachari, K.; Logovinsky, V. *Phys. Rev. Lett.* **1986**, *55*, 2853.
(71) Tomanek, D.; Schlüter, M. A. *Phys. Rev. B* **1987**, *36*, 1208.
(72) Kasper, J. S.; Hagenmuller, P.; Pouchard, M.; Cros, C. *Science* **1965**, *150*, 1713.
(73) Cros, C.; Pouchard, M.; Hagenmuller, P.; Kasper, J. S. *Bull. Soc. Chim. Fr.* **1968**, *7*, 2737.
(74) Cros, C.; Pouchard, M.; Hagenmuller, P. *J. Solid State Chem.* **1970**, *2*, 570.
(75) Cros, C.; Pouchard, M.; Hagenmuller, P. *Bull. Soc. Chim. Fr.* **1971**, *2*, 379.
(76) Roy, S. B.; Sim, K. E.; Caplin, A. D. *Philos. Mag. B* **1992**, *65*, 1445.
(77) Mott, N. F. *J. Solid State Chem.* **1973**, *6*, 348.
(78) Demkov, A. A.; Sankey, O. F.; Schmidt, K. E.; Adams, G. B.; O'Keeffe, M. *Phys. Rev. B* **1994**, *50*, 17001.
(79) Kawaji, H.; Horie, H.; Yamanaka, S.; Ishikawa, M. *Phys. Rev. Lett.* **1995**, *74*, 1427.
(80) Ursenbach, C. P.; Madden, P. A.; Stich, I.; Payne, M. C. *J. Phys. Chem.* **1995**, *99*, 6697.
(81) Jackson, R. A.; Catlow, C. R. A. *Mol. Sim.* **1985**, *1*, 207.
(82) Anderson, P. A.; Edwards, P. P. *J. Am. Chem. Soc.* **1992**, *114*, 10608.
(83) Haug, K.; Srdanov, V. I.; Stucky, G. D.; Matiu, H. *J. Chem. Phys.* **1992**, *96*, 3495.
(84) Srdanov, V. I.; Haug, K.; Matiu, H.; Stucky, G. D. *J. Phys. Chem.* **1992**, *96*, 9039.
(85) Monnier, A.; Srdanov, V. I.; Stucky, G. D.; Matiu, H. *J. Chem. Phys.* **1994**, *100*, 6944.
(86) Blake, N. P.; Srdanov, V. I.; Stucky, G. D.; Matiu, H. *J. Phys. Chem.* **1995**, *99*, 2127.
(87) Nozue, Y.; Kodaire, T.; Goto, T. *Phys. Rev. Lett.* **1992**, *68*, 3789.
(88) Kodaire, T.; Nozue, Y.; Ohwashi, S.; Goto, T.; Terasaki, O. *Phys. Rev. B* **1993**, *B48*, 12245.
(89) Nozue, Y.; Kodaire, T.; Ohwashi, S.; Goto, T.; Terasaki, O. *Phys. Rev. B* **1993**, *48*, 12253.
(90) Chowdhury, A. Z.; Nasu, K. *J. Phys. Chem. Solids* **1995**, *6*, 1183.
(91) Gunnarsson, O. *Phys. Rev. B* **1990**, *41*, 514.
(92) Anisimov, V. I.; Dederichs, P. H. *Solid State Commun.* **1992**, *841*, 241. Anisimov, V. I.; Zaanen, J.; Andersen, O. K. *Phys. Rev. B* **1991**, *44*, 943.
(93) Zhang, Z.; Satpathy, S. *Phys. Rev. B* **1991**, *44*, 13319.

CM9601244